

## High-field magnetization and magnetodielectric effect in a $\text{Ni}_2\text{NbBO}_6$ single crystal

Gaoshang Gong<sup>1,2,3,\*</sup>, Dan Su,<sup>2</sup> Young Sun,<sup>2,4</sup> Longmeng Xu,<sup>5</sup> Jincheng He,<sup>2</sup> and Zhaoming Tian<sup>5,†</sup>

<sup>1</sup>*School of Physics and Electronic Engineering, Zhengzhou University of Light Industry, Zhengzhou 450002, People's Republic of China*

<sup>2</sup>*Beijing National Laboratory for Condensed Matter Physics and Beijing Advanced Innovation Center for Materials Genome Engineering, Institute of Physics, Chinese Academy of Sciences, Beijing 100190, People's Republic of China*

<sup>3</sup>*Henan Key Laboratory of Magneto-electronic Information Functional Materials, Zhengzhou University of Light Industry, Zhengzhou 450002, People's Republic of China*

<sup>4</sup>*Center of Quantum Materials and Devices, Chongqing University, Chongqing 401331, People's Republic of China*

<sup>5</sup>*School of Physics and Wuhan National High Magnetic Field Center, Huazhong University of Science and Technology, Wuhan 430074, People's Republic of China*



(Received 13 September 2021; revised 20 December 2021; accepted 18 January 2022; published 10 February 2022)

We have studied the magnetization, dielectric permittivity, thermal expansion, and magnetostriction of  $\text{Ni}_2\text{NbBO}_6$  single crystals. Different from that of the  $ab$  plane, the  $c$  axis magnetization approaches zero at low magnetic fields and a spin-flop transition happens around  $H_{\text{SF}} = 3.65$  T. The results indicate that the  $c$  axis is the hard axis and the  $ab$  plane is the easy plane. The high-field isothermal magnetization measured at  $T = 4.2$  K reveals that the saturation magnetic field is  $H_s = 17$  T, above which the magnetic structure changes from canted-antiferromagnetic order to ferromagnetic order with the saturation magnetic moment  $\mu_{\text{eff}} = 2.40 \mu_{\text{B}}/\text{Ni}^{2+}$ . Below antiferromagnetic transition temperature  $T_N$ , an unusual negative thermal expansion phenomenon is detected along the  $b$  axis and it can be interpreted by the magnetic structural variation. Based on the magnetization and the magnetostriction data, the magnetic field–temperature phase diagram of  $\text{Ni}_2\text{NbBO}_6$  is constructed. The magnetodielectric effect confirms the existence of magnetoelectric coupling in  $\text{Ni}_2\text{NbBO}_6$ .

DOI: [10.1103/PhysRevB.105.054408](https://doi.org/10.1103/PhysRevB.105.054408)

### I. INTRODUCTION

The concept of frustration has been applied broadly, from negative thermal expansion solids to soft materials [1]. For magnetism, a variety of interesting properties and exotic magnetic ground states exist in frustrated magnets [2–6]. The square, triangular, and kagome lattices; zigzag chains; Kitaev magnets; and frustrated spin-ice magnets have attracted great interest [7–9]. Among them, the low-dimensional antiferromagnetic insulator  $\text{Ni}_2\text{NbBO}_6$ , which was first synthesized about four decades ago, has been investigated extensively in recent years [10–13]. As drawn in Fig. 1(a), it crystallizes into an orthorhombic structure with the  $pnma$  space group [13]. Along the  $c$  axis, the lattice can be viewed as a zigzag spin chain. Alternatively, along the  $b$  axis, double edge shared  $[\text{NiO}_6]$  octahedra are linked by the  $[\text{NbO}_6]$  octahedra and  $[\text{BO}_4]$  tetrahedra [11]. The nonmagnetic borate anions allow the transmission of magnetic interactions via a super-superexchange route [14–16], leading to the formation of a  $S = 1$  low-dimensional armchair spin chain system [see Fig. 1(b)] [17,18]. Below the antiferromagnetic transition temperature  $T_N \sim 23.5$  K, a sizable interchain coupling happens in  $\text{Ni}_2\text{NbBO}_6$  and it results in the establishment of long-range antiferromagnetic spin ordering [12]. As Fig. 1(b) shows, the neighbor red-red color or blue-blue color magnetic

moment of  $\text{Ni}^{2+}$  ions are ferromagnetically coupled as a  $S = 1$  dimer along the  $b$  direction, while the interdimer interactions are antiferromagnetic within the armchair chains. According to previous reports, the  $a$  direction is the anisotropic easy axis. While a magnetic field is applied along this axis, an obvious field-induced spin-flop transition occurs around  $H_{\text{SF}} = 3.65$  T at  $T = 2$  K [13], but according to the literature, the maximal applied field is  $H_{\text{max}} = 7$  T, much lower than the saturation field of  $\text{Ni}_2\text{NbBO}_6$ . As the high magnetic field is an effective way to characterize the antiferromagnetic system [19], in this paper it was employed to investigate the magnetic structure of a  $\text{Ni}_2\text{NbBO}_6$  single crystal. Based on the measurement results, the  $c$  axis is proposed to be the spin-flop transition axis instead of the reported  $a$  axis. The obtained saturation magnetic moment and saturation field from the high-field magnetization measurements can be important parameters to determine the interaction strength in this compound. The magnetic field–temperature ( $H$ - $T$ ) phase diagram is constructed, laying a solid foundation for understanding this material.

Additionally, the magnetodielectric effect is one fascinating and auspicious phenomenon in both scientific and technological aspects for potential applications [20–24]. The existence of the spin-flop transition in  $\text{Ni}_2\text{NbBO}_6$  indicates that the antiferromagnetic moment can be reversed by an external field. In this special case, typical spin-lattice coupling, and thus strong magnetodielectric effect may be expected [25,26]. To confirm these effects, the magnetostriction and dielectric properties of  $\text{Ni}_2\text{NbBO}_6$  are also investigated.

\* gonggaoshang@zzuli.edu.cn

† tianzhaoming@hust.edu.cn

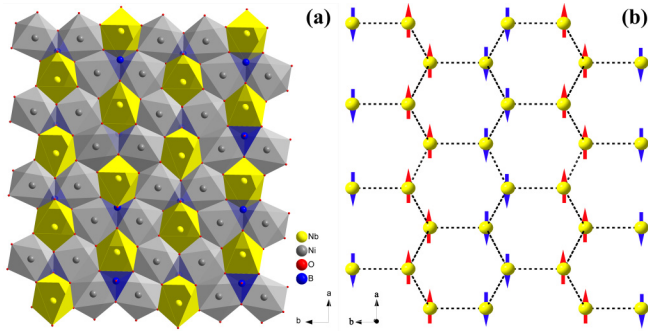


FIG. 1. (a) The crystal structure of  $\text{Ni}_2\text{NbBO}_6$ , viewing along the  $c$  direction; (b) the reported armchair spin arrangement of  $\text{Ni}^{2+}$  ions.

## II. EXPERIMENTAL DETAILS

The  $\text{Ni}_2\text{NbBO}_6$  single crystal was prepared by the flux-melt method as described elsewhere [13]. The crystal structure was checked by powder x-ray diffractions (XRD) (Philips X'Pert Pro) using the  $\text{Cu } K\alpha$  radiation x ray of  $\lambda = 1.5401 \text{ \AA}$ . The structural refinement was performed with MATERIALS STUDIO software. The low-field magnetization was measured by a commercial physical properties measurement system (Quantum Design, Dynacool II). The pulsed high-field magnetization was measured at Wuhan National High Magnetic Field Center, Huazhong University of Science and Technology. The thermal expansion coefficient  $\Delta L/L$  and magnetostriction were measured with a capacitance dilatometer. The permittivity for the  $E//a$   $E//a$  direction was measured with an Andeen Hagerling 2700A capacitance bridge and the applied frequency was 20 kHz. The permittivity for the  $E//c$  direction was measured with an Agilent 4980 LCR meter.

## III. RESULTS AND DISCUSSION

Figure 2 shows the refined XRD pattern of  $\text{Ni}_2\text{NbBO}_6$  powder. All the diffraction peaks are indexed to the or-

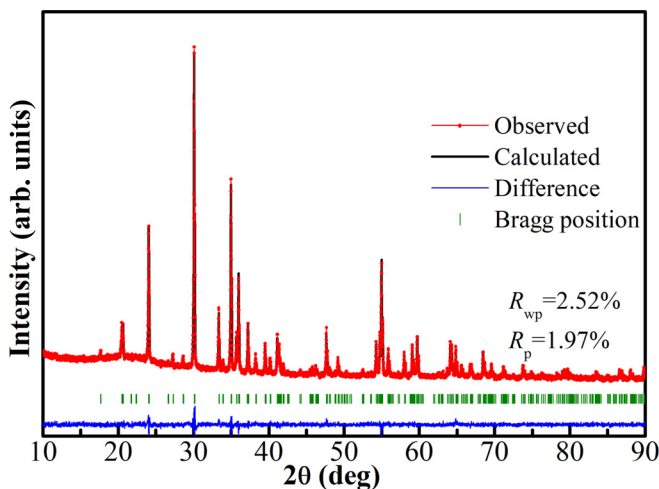


FIG. 2. The XRD patterns of  $\text{Ni}_2\text{NbBO}_6$  powder. The blue solid line shows the difference between the observed value and the calculated value.

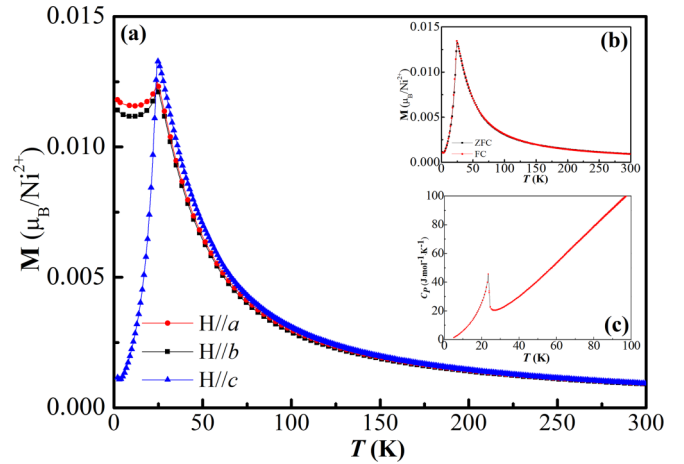


FIG. 3. (a) The ZFC  $M$ - $T$  curves measured along different crystallographic directions with  $H = 0.1 \text{ T}$ . (b) The ZFC and FC curves for  $H//c$  axis. (c) Temperature dependence of specific heat of a  $\text{Ni}_2\text{NbBO}_6$  single crystal.

thorhombic structure (space group  $Pnma$ ) and no impurity phase is detected. The obtained refinement parameters  $R_{wp}$  and  $R_p$ , equal to 2.52% and 1.97%, respectively, confirm the high quality of the present sample. The calculated lattice parameters  $a = 10.057 \text{ \AA}$ ,  $b = 8.618 \text{ \AA}$ ,  $c = 4.490 \text{ \AA}$  are also consistent with a previous report [13].

The zero field cooling (ZFC) magnetization for all three crystallographic axes is measured and the results are shown in Fig. 3(a). Around  $T = 23.5 \text{ K}$ , a sharp peak exists. Simultaneously, the field cooling (FC) magnetization for the  $H//c$  direction and the specific heat are also characterized. The completely overlapped ZFC and FC curves as shown in Fig. 3(b) together with the  $\lambda$ -shaped specific heat peak as shown in Fig. 3(c) well confirm the antiferromagnetic phase transition of  $\text{Ni}_2\text{NbBO}_6$ . But differently, instead of the reported results that the  $a$  axis is the hard axis, i.e., below the antiferromagnetic transition temperature  $T_N$  the susceptibility of the  $H//a$  axis condition is much lower than the  $H//bc$ -plane case, the present measurement results indicate that the  $c$  axis is the hard axis of the  $\text{Ni}_2\text{NbBO}_6$  single crystal and the  $ab$  plane is the easy plane.

To clarify the magnetic structure, the isothermal magnetization ( $M$ - $H$ ) curves of a  $\text{Ni}_2\text{NbBO}_6$  single crystal are measured. Figure 4(a) gives the  $M$ - $H$  curves that were measured with the commercial physical properties measurement system. Due to the instrument limit, the maximal applied field is only 7 T. To characterize the high-field magnetization, a pulsed field was employed and the obtained data were drawn in Fig. 4(b). Figures 4(c)–4(e) show the comparison of the magnetization measured with two different methods. From both Figs. 4(a) and 4(b) it is noticed that for a magnetic field parallel to the  $a$  or  $b$  axis, the magnetization increases linearly at low field with the field. For the  $H//c$  direction, the low-field magnetization approaches zero. As the field increases, the magnetization presents a sudden jump around  $H_{SF} = 3.65 \text{ T}$ , manifesting that a spin-flop transition happens. Subsequently, the  $c$  axis displays similar behavior with the  $a$  and  $b$  axes. Namely, due to the antiferromagnetic feature,

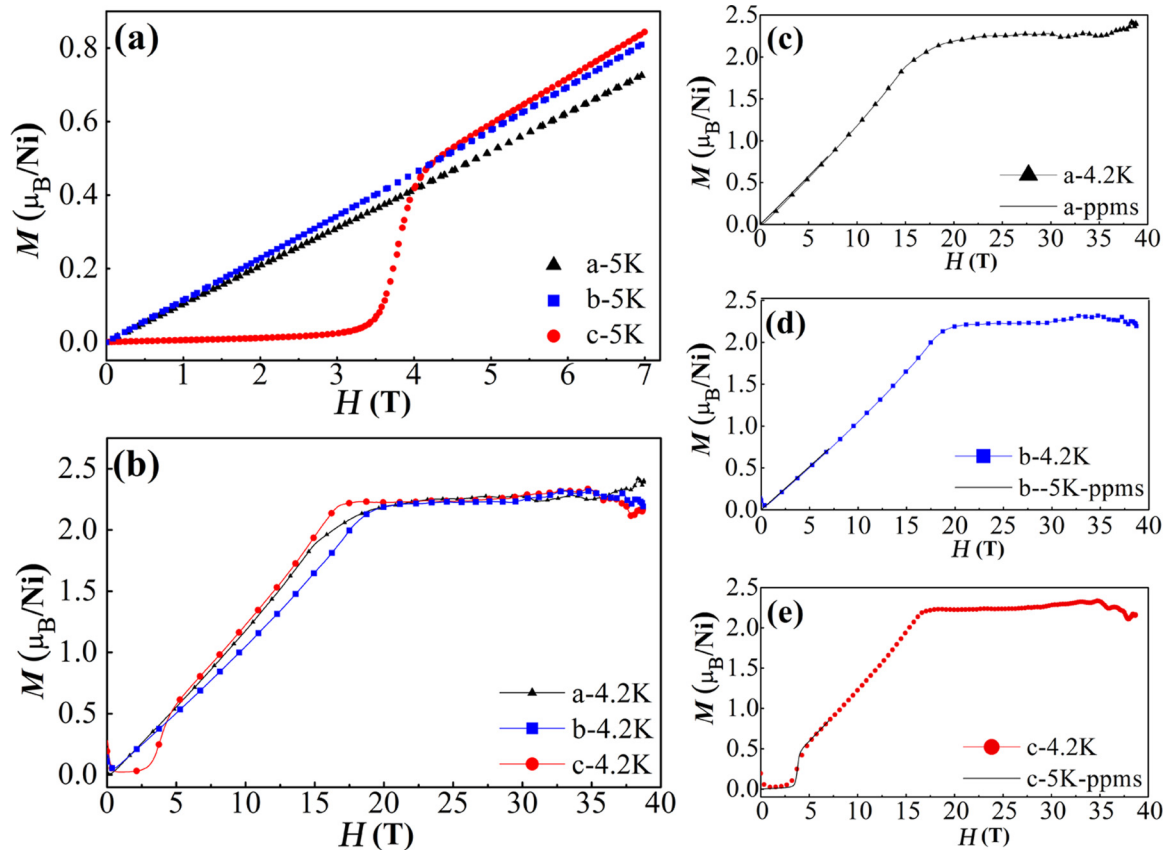


FIG. 4. (a) The isothermal magnetization ( $M$ - $H$ ) curves of a  $\text{Ni}_2\text{NbBO}_6$  single crystal measured with commercial physical properties measurement system along different crystalline directions. (b) The  $M$ - $H$  curves of a  $\text{Ni}_2\text{NbBO}_6$  single crystal measured by pulsed field up to 40 T. (c)–(e) The comparison of magnetization measured with a commercial physical properties measurement system and pulsed field facility.

the magnetization increases linearly in the range of 4–17 T and finally it becomes saturated around the saturation field  $H_s = 17$  T. As shown in Fig. 4(b), for all the crystal axes the saturation magnetic moment for  $\text{Ni}^{2+}$  is  $\mu_{\text{eff}} = 2.40 \mu_B$ . This value is slightly lower than the calculated spin-only value for the  $S = 1$  ( $\mu_{\text{cal}} = 2.83 \mu_B$ ) system. The obtained saturation magnetic moment and saturation field  $H_s$  from the high-field magnetization measurements can be important parameters to determine the interaction strength in this compound.

From the variation of the magnetization shown in Figs. 4(a) and 4(b), it is reasonable to speculate that for the ground state of  $\text{Ni}_2\text{NbBO}_6$  the spins are aligned in the  $ab$  plane. Therefore, while a magnetic field is applied along the  $a$  or  $b$  axis, the spins can be reversed to the parallel or antiparallel direction of external field easily and a linear increase of magnetization is observed. But it is hard to reverse the spins to the  $\pm c$  direction, which is perpendicular to the  $ab$  plane. As a result, if the magnetic field is parallel to the  $c$  axis and it is lower than the critical field  $H_{\text{SF}}$ , the magnetization is almost zero. Around  $H_{\text{SF}}$ , the spins switch from the  $ab$  plane to the  $\pm c$  direction by the benefit of an external field and a sudden jump of magnetization is caused. Accompanying this process, the  $\text{Ni}_2\text{NbBO}_6$  evolves to canted antiferromagnetic structure. At high field, the saturation magnetization indicates that a field-induced transition from canted antiferromagnetic state to ferromagnetic state occurs at saturation field  $H_s$ ; above that all the spins are parallel to the direction of the external field.

According to the above discussion, the  $c$  axis is the hard axis. To investigate the unique spin-flop behavior of a  $\text{Ni}_2\text{NbBO}_6$  single crystal, a field parallel to the  $c$  axis is applied and the  $M$ - $H$  curves were measured at different temperatures. As Fig. 5(a) shows, the temperature greatly influences the spin-flop field  $H_{\text{SF}}$  and the saturation field  $H_s$ . For comparing intuitively, the  $dM/dH$  curves are drawn in Fig. 5(b). With the temperature increases both the  $H_{\text{SF}}$  and  $H_s$  decrease. Above the antiferromagnetic transition temperature  $T_N$ , there is no anomaly in the  $dM/dH$  curves can be observed, demonstrating the disappearance of the spin-flop phenomenon accompanying the magnetic moment becoming disorderly.

The variation of the magnetic structure usually leads to the change of crystal volume. Here, a high-resolution capacitance dilatometer was employed to measure the expansion of the  $\text{Ni}_2\text{NbBO}_6$  single crystal. For the capacitance dilatometer, a small variation in sample length can be transformed into a change in capacitance. The calculated expansion coefficient that is defined as  $[L(T) - L(5 \text{ K})]/L(5 \text{ K})$  is shown in Fig. 6(a). In the high-temperature region, along both the  $b$  and  $c$  axes the  $\text{Ni}_2\text{NbBO}_6$  shrinks slightly with decreasing temperature. Below the antiferromagnetic transition temperature  $T_N$ , however, the two directions present different behaviors. The  $\Delta L/L$  value of the  $c$  axis decreases more rapidly with lowering temperature, while the  $\Delta L/L$  value of the  $b$  axis increases slightly [see the inset of Fig. 6(a)]. The anomaly of the expansion coefficient around  $T_N$  suggests that the lattice

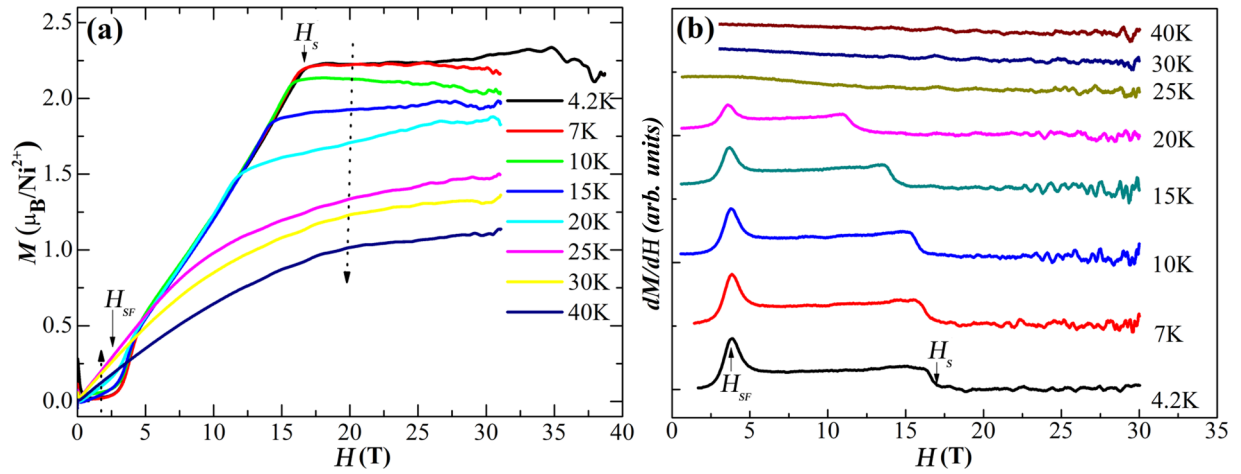


FIG. 5. The isothermal magnetization along the  $c$  axis of a  $\text{Ni}_2\text{NbBO}_6$  single crystal measured at different temperatures. The dotted arrows indicate the ordering of these curves. (b) The  $dM/dH$  curves at different temperatures. The curves are shifted upward for comparison. The arrows denote the spin-flop fields  $H_{\text{SF}}$  and the saturation magnetic field  $H_s$ .

structure is affected by the magnetic structural change, confirming the magnetic-lattice coupling of  $\text{Ni}_2\text{NbBO}_6$ . The negative thermal expansion coefficient along the  $b$  axis of  $\text{Ni}_2\text{NbBO}_6$  is unusual and it may be explained by the magnetization variation. In the paramagnetic state, the spins rank to all directions randomly. Due to the heat-expansion and cold-contraction effect, cooling the sample makes the  $\Delta L/L$  value of all the directions decrease. At  $T_N$ , the magnetic structure changes to antiferromagnetic order. The transition from paramagnetic state to antiferromagnetic state results in the spins lying in the  $ab$  plane. The shift of spins from the  $c$  direction to the  $ab$  plane accelerates the shrinkage of the  $c$  axis and makes the  $b$  axis expand.

Figure 6(b) shows the magnetic field dependent magnetostriction coefficient along the  $b$  and  $c$  axes. At  $T = 25$  K, which is above the antiferromagnetic transition temperature  $T_N$ , the  $\Delta L/L$  decreases slightly with applied magnetic fields. Below  $T_N$ , the  $\Delta L/L$  along both the  $b$  and  $c$  directions increases with increasing low magnetic field. As the field increases further, a reduced tendency in the high-field region can be observed. The corresponding magnetic field of the maximum of the  $d(\Delta L)/dH$  curve is equal to the critical field  $H_{\text{SF}}$  [as the blue line shows in Fig. 6(c)], implying that the expansion of the lattice is caused by the flop of the spin to the magnetic field direction. The result is in accordance with the temperature-dependent expansion curves, i.e.,

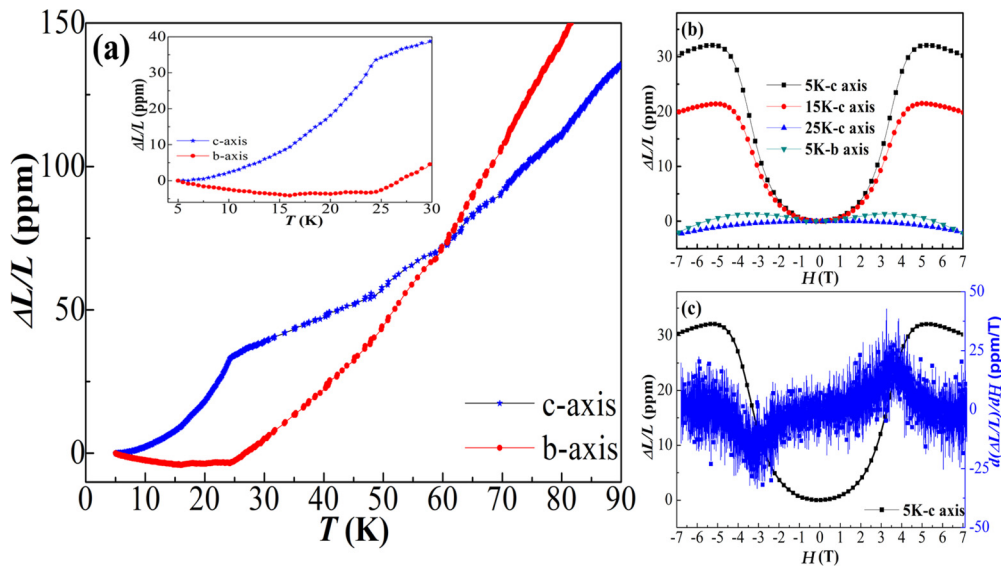


FIG. 6. (a) Temperature dependence of the thermal expansion of a  $\text{Ni}_2\text{NbBO}_6$  single crystal along the  $b$  and  $c$  axes. The value of  $\Delta L/L$  was normalized as  $[L(T) - L(5\text{K})]/L(5\text{K})$ ; the inset shows the zoomed-in view of the low-temperature region. (b) Magnetostriction coefficient  $[L(H) - L(0T)]/L(0T)$  along different axes of  $\text{Ni}_2\text{NbBO}_6$  measured at different temperatures. (c) Magnetostriction along the  $c$  axis measured at  $T = 5$  K and its differential to the magnetic field.

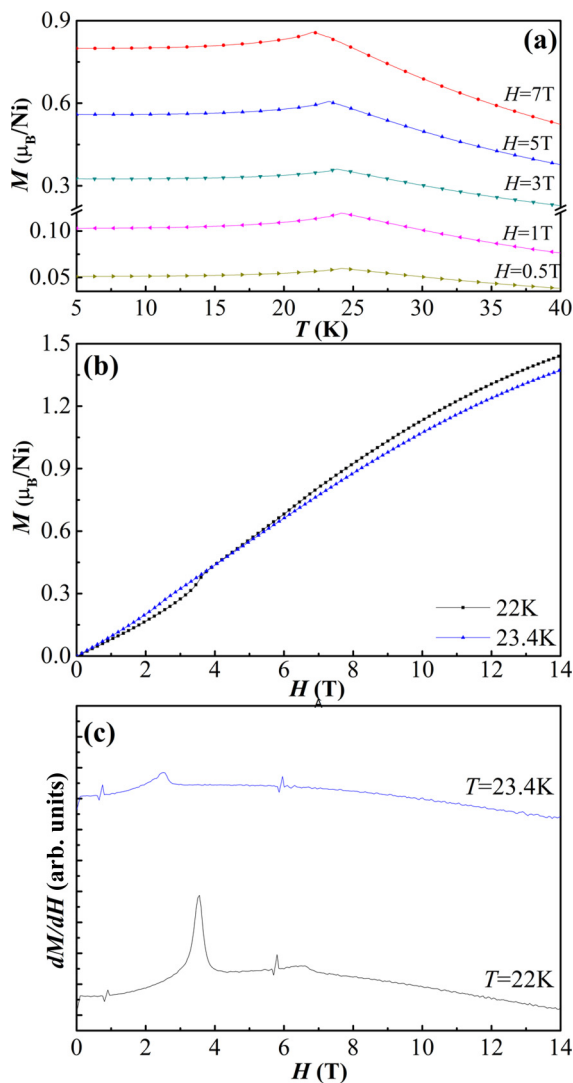


FIG. 7. (a) The zero field cooling magnetization of a  $\text{Ni}_2\text{NbBO}_6$  single crystal measured under different fields, (b) the isothermal magnetization  $M$ - $H$  curves, and (c)  $dM/dH$  curves of  $\text{Ni}_2\text{NbBO}_6$  measured at  $T = 22\text{ K}$  and  $T = 23.4\text{ K}$ ; the magnetic field is parallel to the  $c$  axis.

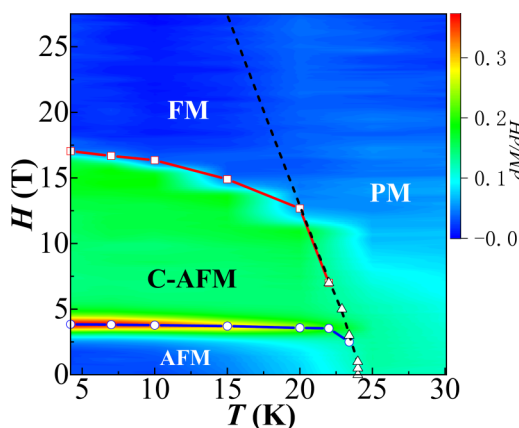


FIG. 8. Magnetic field-temperature ( $H$ - $T$ ) phase diagram of  $\text{Ni}_2\text{NbBO}_6$ .

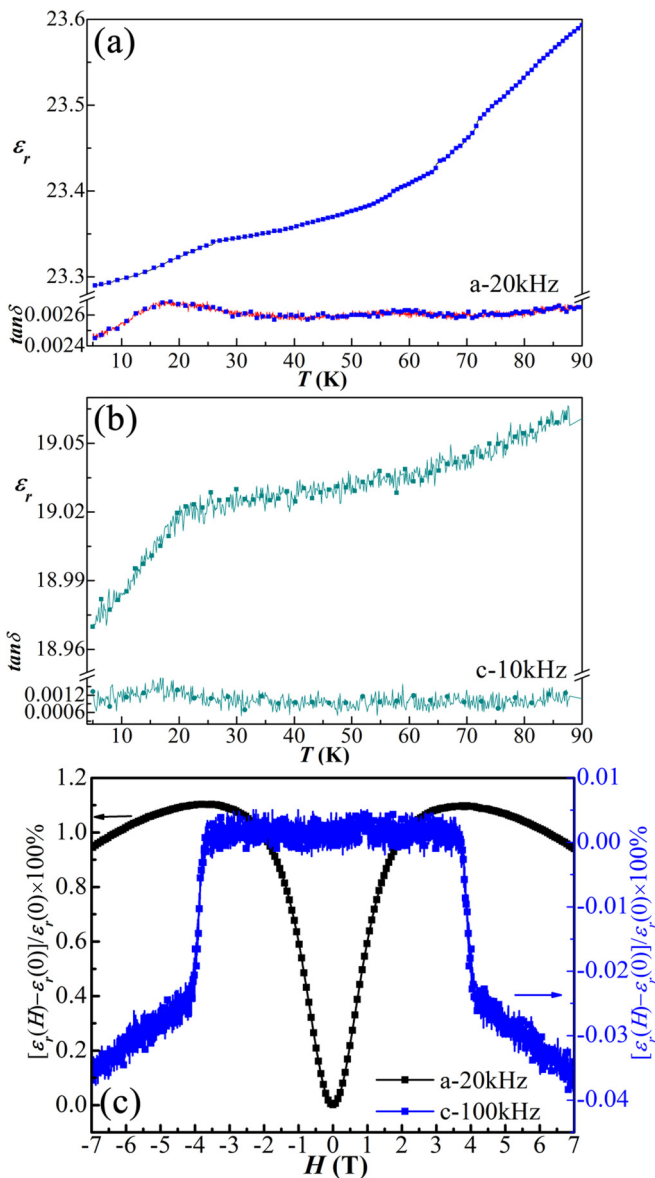


FIG. 9. The temperature dependence of dielectric permittivity and loss of a  $\text{Ni}_2\text{NbBO}_6$  single crystal measured with (a)  $E//a$  axis and (b)  $E//c$  axis. (c) The magnetodielectric effect measured at  $5\text{ K}$  with  $H//E//a$  axis and  $H//E//c$  axis.

the direction in which the spin flop to that dimension will expand .

Based on the high-field magnetization, thermal expansion curves, and magnetic field and temperature-dependent low-field magnetization (see Fig. 7), the  $H$ - $T$  phase diagram of the  $\text{Ni}_2\text{NbBO}_6$  single crystal can be constructed (Fig. 8). For a magnetic field parallel to the  $c$  axis, the antialigned spins lie in the  $ab$  plane at low fields. As the field increases to  $H_{SF}$ , the spins flop to the  $c$  axis and canted antiferromagnetic order forms. Around the saturation field  $H_s = 17\text{ T}$ , all the magnetic moments are reversed to the magnetic field direction and the magnetization becomes saturated.

Figures 9(a) and 9(b) present the temperature dependence of dielectric permittivity and loss of the  $\text{Ni}_2\text{NbBO}_6$  single crystal for  $E//a$  axis and  $E//c$  axis, respectively. With the

magnetic structure changing from disorder to order, an obvious dielectric anomaly appears around  $T_N$  for both directions. It verifies the magnetic-dielectric coupling of the  $\text{Ni}_2\text{NbBO}_6$  single crystal. The coupling can be also confirmed by the magnetic field dependence of dielectric permittivity. Figure 9(c) shows the normalized magnetic field dependent dielectric permittivity measured at 5 K with the  $H//E//a$  axis and the  $H//E//c$  axis. Below the spin-flop field  $H_{\text{SF}}$ , the spins lie in the  $ab$  plane with antiferromagnetic order. Application of a magnetic field along the  $a$  axis results in the increase of the dielectric permittivity. The magnitude of the magnetodielectric effect can reach 1.10%. In contrast, the dielectric permittivity measured under  $H//E//c$  condition does not change below  $H_{\text{SF}}$  because there is no magnetic moment along the  $c$  axis. Above  $H_{\text{SF}}$ , as the magnetic field increases, the permittivity decreases for both the  $H//E//a$  axis and the  $H//E//c$  axis. In particular, for the  $H//E//c$  axis case, the spin flop to the  $c$  axis around  $H_{\text{SF}}$  makes the permittivity decrease suddenly. Though the variation is lower than 0.04%, it is still larger than those reported in some magnetic oxides, such as  $\text{NiCr}_2\text{O}_4$  (0.02%) [27,28] and  $\text{CoCr}_2\text{O}_4$  (0.01%) [27].

#### IV. CONCLUSIONS

A  $\text{Ni}_2\text{NbBO}_6$  single crystal was synthesized by the flux-melt method. Magnetization measurement indicates that the  $c$

axis is the hard axis instead of the reported  $a$  axis. Around the saturation magnetic field  $H_s = 17$  T, a field-induced magnetic phase transition from canted-antiferromagnetic order to ferromagnetic order happens. The thermal expansion and magnetostriction are discussed in terms of the magnetic structural variation. After the transition from paramagnetic to antiferromagnetic state, the spins become ordered in the  $ab$  plane, which makes the sample expand along the  $b$  axis. When a field is applied along the  $c$  axis, the spins flop to the  $c$  direction around  $H_{\text{SF}} = 3.65$  T, and the sample expands along the  $c$  axis. Based on the magnetization and expansion measurements, the magnetic field temperature phase diagram of  $\text{Ni}_2\text{NbBO}_6$  is constructed, laying a solid foundation for understanding this material. The temperature and magnetic field dependent dielectric permittivity confirms the magnetodielectric coupling of the  $\text{Ni}_2\text{NbBO}_6$  single crystal.

#### ACKNOWLEDGMENTS

This work was supported by the Key Research Project of Colleges and Universities of Henan Province (Grant No. 20A140029), the Research Project of Department of Science and Technology of Henan Province (Grant No. 212102210477), and the National Natural Science Foundation of China (Grant No. 11874158).

- 
- [1] L. Balents, Spin liquids in frustrated magnets, *Nature (London)* **464**, 200 (2010).
- [2] S. T. Bramwell and M. J. P. Gingras, Spin ice state in frustrated magnetic pyrochlore materials, *Science* **294**, 1495 (2001).
- [3] Y. Shimizu, K. Miyagawa, K. Kanoda, M. Maesato, and G. Saito, Spin Liquid State in an Organic Mott Insulator with a Triangular Lattice, *Phys. Rev. Lett.* **91**, 107001 (2003).
- [4] A. Maity, Y. Iqbal, and S. Mandal, Competing orders in a frustrated Heisenberg model on the Fisher lattice, *Phys. Rev. B* **102**, 224404 (2020).
- [5] G. Pokharel, H. S. Arachchige, T. J. Williams, A. F. May, R. S. Fishman, G. Sala, S. Calder, G. Ehlers, D. S. Parker, T. Hong, A. Wildes, D. Mandrus, J. A. M. Paddison, and A. D. Christianson, Cluster Frustration in the Breathing Pyrochlore Magnet  $\text{LiGaCr}_4\text{S}_8$ , *Phys. Rev. Lett.* **125**, 167201 (2020).
- [6] H. C. Zhao, J. H. Zhang, M. Lyu, S. Bachus, Y. Tokiwa, P. Gegenwart, S. Zhang, J. G. Cheng, Y. F. Yang, G. F. Chen, Y. Isikawa, Q. M. Si, F. Steglich, and P. J. Sun, Quantum-critical phase from frustrated magnetism in a strongly correlated metal, *Nat. Phys.* **15**, 1261 (2019).
- [7] R. Samajdar, W. W. Ho, H. s Pichler, M. D. Lukin, and S. Sachdev, Complex Density Wave Orders and Quantum Phase Transitions in a Model of Square-Lattice Rydberg Atom Arrays, *Phys. Rev. Lett.* **124**, 103601 (2020).
- [8] M. G. Gonzalez, E. A. Ghioldi, C. J. Gazza, L. O. Manuel, and A. E. Trumper, Interplay between spatial anisotropy and next-nearest-neighbor exchange interactions in the triangular Heisenberg model, *Phys. Rev. B* **102**, 224410 (2020).
- [9] H. Y. Zou, E. H. Zhao, X. W. Guan, and W. V. Liu, Exactly Solvable Points and Symmetry Protected Topological Phases of Quantum Spins on a Zig-Zag Lattice, *Phys. Rev. Lett.* **122**, 180401 (2019).
- [10] B. M. Wanklyn, F. R. Wondre, and W. Davison, Flux growth of crystals of some magnetic oxide materials:  $\text{Mn}_7\text{SiO}_{12}$ ,  $\text{CuO}$ ,  $\text{MCr}_2\text{O}_4$ ,  $\text{MTiO}_3$ ,  $\text{Ni}_2\text{NbBO}_6$ ,  $\text{MMoO}_4$ , and  $\text{Li}_2\text{M}_2(\text{MoO})_4$ , ( $M = \text{Mn, Co, Ni}$ ), *J. Mater. Sci.* **11**, 1607 (1976).
- [11] G. B. Ansell, M. E. Leonowicz, M. A. Modrick, B. M. Wanklyn, and F. R. Wondre, The structure of dinickel niobium (V) boron oxide  $\text{Ni}_2\text{NbBO}_6$ , *Acta Crystallogr., Sect. B* **38**, 892 (1982).
- [12] M. A. Prosnikov, A. N. Smirnov, V. Yu. Davydov, and R. V. Pisarev, Magnetic dynamics and spin-phonon coupling in the antiferromagnet  $\text{Ni}_2\text{NbBO}_6$ , *Phys. Rev. B* **98**, 104404 (2018).
- [13] G. Narsinga Rao, V. N. Singh, R. Sankar, I. Panneer Muthuselvam, G. Y. Guo, and F. C. Chou, Antiferromagnetism of  $\text{Ni}_2\text{NbBO}_6$  with  $S = 1$  dimer quasi-one-dimensional arm-chair chains, *Phys. Rev. B* **91**, 014423 (2015).
- [14] S. R. White and I. Affleck, Dimerization and incommensurate spiral spin correlations in the zigzag spin chain: Analogies to the Kondo lattice, *Phys. Rev. B* **54**, 9862 (1996).
- [15] T. Hikihara, M. Kaburagi, H. Kawamura, and T. Tonegawa, Ground state phase diagram of frustrated  $S = 1$   $XXZ$  chains: Chiral ordered phases, *J. Phys. Soc. Jpn.* **69**, 259 (2000).
- [16] A. Kolezhuk, R. Roth, and U. Schollwock, First Order Transition in the Frustrated Antiferromagnetic Heisenberg  $S = 1$  Quantum Spin Chain, *Phys. Rev. Lett.* **77**, 5142 (1996).
- [17] R. Borromei and E. Caval, Low-temperature absorption spectrum of  $\text{Ni}^{2+}$  ion in single crystals of  $\text{Ni}_2\text{NbBO}_6$ , *Phys. Status Solidi B* **123**, 679 (1984).

- [18] M. Prosnikov, S. Bariho, N. Lyubochko, S. Shiryaev, A. Smirnov, V. Davydov, and R. Pisarev, Magnetic Raman scattering and symmetry analysis of complex-structure antiferromagnets  $\text{Ni}_2\text{NbBO}_6$  and  $\text{Fe}_3\text{BO}_6$ , *Acta Crystallogr., Sect. A* **74**, e332 (2018).
- [19] M. Y. Ruan, Z. W. Ouyang, S. S. Sheng, X. M. Shi, Y. M. Guo, J. J. Cheng, and Z. C. Xia, High-field magnetization and ESR studies of spin-chain compound  $\text{Ca}_3\text{CoMnO}_6$ , *J. Magn. Magn. Mater.* **344**, 55 (2013).
- [20] Y. Cao, N. Kobayashi, S. Ohnuma, and H. Masumoto, Large tunneling magneto-dielectric enhancement in  $\text{Co}(\text{Fe})\text{-MgF}_2$  granular films by minor addition of Si, *Appl. Phys. Lett.* **117**, 072904 (2020).
- [21] V. K. Anusree, P. N. Lekshmi, S. G. Bhat, A. A. Wagh, G. Das, and P. N. Santhosh, Dielectric relaxation, magneto-dielectric coupling, and pyrocurrent anomaly in point defect controlled  $\text{HoCrO}_3$ , *J. Appl. Phys.* **127**, 194105 (2020).
- [22] R. Mandal, M. Chandra, V. Roddatis, P. Ksoll, M. Tripathi, R. Rawat, R. J. Choudhary, and V. Moshnyaga, Magneto-dielectric effect in relaxor superparaelectric  $\text{Tb}_2\text{CoMnO}_6$  film, *Phys. Rev. B* **101**, 094426 (2020).
- [23] Z. L. Zheng, X. Wu, Q. Y. Feng, and V. G. Harris, Low loss and tailored high-frequency performances of BaO-doped  $\text{NiZnCo}$  magneto-dielectric ferrites, *J. Am. Ceram. Soc.* **103**, 1248 (2020).
- [24] H. Y. Zhao, H. Kimura, Z. X. Cheng, M. Osada, J. L. Wang, X. L. Wang, S. X. Dou, Y. Liu, J. D. Yu, T. Matsumoto, T. Tohei, N. Shibata, and Y. Ikuhara, Large magnetoelectric coupling in magnetically short-range ordered  $\text{Bi}_5\text{Ti}_3\text{FeO}$  film, *Sci. Rep.* **4**, 5255 (2014).
- [25] T. Kolodiaznyy, H. Sakurai, and N. Vittayakorn, Spin-flop driven magneto-dielectric effect in  $\text{Co}_4\text{Nb}_2\text{O}$ , *Appl. Phys. Lett.* **99**, 132906 (2011).
- [26] T. Kolodiaznyy and H. Sakurai, Electronic, thermoelectric, and magneto-dielectric properties of  $\text{Ca}_{1-x}\text{Na}_x\text{Cr}_2\text{O}_4$ , *J. Appl. Phys.* **113**, 224109 (2013).
- [27] N. Mufti, A. A. Nugroho, G. R. Blake, and T. T. M. Palstra, Magnetodielectric coupling in frustrated spin systems: The spinels  $\text{MCr}_2\text{O}_4$  ( $\text{M} = \text{Mn}, \text{Co}$  and  $\text{Ni}$ ), *J. Phys.: Condens. Matter* **22**, 075902(2010).
- [28] T. D. Sparks, M. C. Kemei, P. T. Barton, and R. Seshadri, Magnetocapacitance as a sensitive probe of magnetostructural changes in  $\text{NiCr}_2\text{O}_4$ , *Phys. Rev. B* **89**, 024405 (2014).